An Efficient Speed Function for Segmentation of GBM in MRI Images Based on Level set Method

Alireza Mojtabavi, Parastoo Farnia, Alireza Ahmadian*, Hamidreza Saligheh Rad
Image-Guided Surgery Group, Research Center of Biomedical Technology and Robotics RCBTR
Tehran University of Medical Sciences
Tehran, Iran.

Meysam Alimohamadi, Ahmad Pourrashidi
Sina Specialized & Subspecialty Hospital
Tehran University of Medical Sciences
Tehran, Iran.

***Abstract*—Accurate segmentation and characterization of abnormalities in brain tumor are challenging task, especially in the case of GBM tumors, where the ambiguities presented in the boundaries of these tumors necessitates using efficient segmentation method.**

Level set methods have proven to be a flexible and powerful tool for image segmentation because of being shape-driven method with a properly defined speed function to grow or shrink the boundaries to segment complex objects of interest, precisely.

In this study a combined level set algorithm consists of both region and boundary terms for GBM segmentation is proposed. The modified speed function incorporates threshold based level set and the Laplacian filter to highlight the fine details for performing an accurate extraction of the tumor region using multiple seed points selected by the user.

An evaluation was performed on a dataset containing 6 patients with GBM by using three measures Dice, False Positive Error (FPE) and False Negative Error (FNE). Manual segmentation of GBM is considered as gold standard. Compared to traditional method, the mean of FPE and FNE are improved by 53.5% and 53.1%, respectively. The mean of Dice coefficients between our results and gold standard measurement reached to 0.88.

As the results proved, the proposed combined method improves the accuracy of GBM segmentation by 16% compared to conventional threshold based level set method. The proposed method is also robust to change of parameters.

Keywords- semi-automatic segmentation; GBM; Level set;

I. INTRODUCTION

Segmentation of a brain tumor in magnetic resonance images (MRI) has a crucial role in medical diagnosis, since it provides information associated with anatomical structures as well as potential abnormal tissues necessary to treatment planning and patient follow-up [1]. Brain tumors consist of different tissues such as necrosis, active tumor and edema (Fig.1). Extraction of active tumor boundary is an important part of treatment planning. The accurate estimation of tumor boundary (active tumor) is a challenging and difficult task because of the variety of the possible shapes, locations and image intensities of tumors [1] while it is substantial for clinical reasons, e.g., for treatment planning and therapy evaluation [2].

Glioblastoma multiforme (GBM), which is a Grade IV brain tumor according to the World Health Organization (WHO) classification, is the most common form of primary brain tumor in the central nervous system (CNS), and its aggressive nature and evasiveness make it one of the most lethal cancers to treatments [3]. The incidence of GBM is estimated at 3.20 per 100,000 individuals per year. Globlastoma account for 14.9% of all primary brain and other CNS tumors and is the most frequent malignant primary brain tumor, representing 46.6% of all malignant CNS tumors [4].

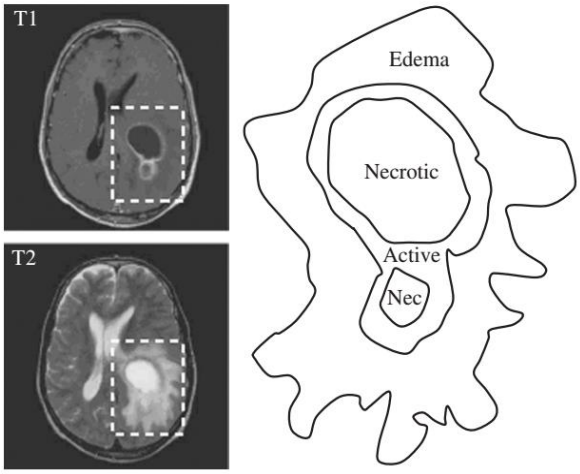

Figure.1 Labeled example of a brain tumor in the T1 with contrast and T2 modalities (adapted from [5])

Treatment protocols for malignant brain tumors generally call for removal through surgical procedures of the tumor. The goal of surgery is to remove the tumor without causing damage to the surrounding normal tissues. Achieving this goal requires accurate tumor segmentation [6].

Brain tumor segmentation methods can be classified into three categories according to the degree of human interaction: manual, semi-automatic, and fully automatic segmentation [5].

The manual brain tumor segmentation is generally a challenging and time-consuming task. Fully automated segmentation techniques improve constantly; however, automated image analysis technique cannot apply fully

autonomously with guaranteed results in the general case. Reluctance to embrace the fully automatic approach may be due to the concerns about its insufficient reliability in cases where the target anatomy may differ from the norm [7]. That is why semi-automatic segmentation techniques, which allow solving moderate and hard segmentation tasks by modest user effort, become more and more popular. Interactive segmentation can provide effective control to the surgeon and increase the efficiency and robustness of segmentation.

Several algorithms have already been proposed for semi-automatic brain tumor segmentation, which rely on magnetic resonance imaging. Boykov et al. [8] have presented a segmentation approach that uses GraphCut, which is a combinatorial optimization technique applied to image segmentation. Since then, many varied methods based on this algorithm have been developed [9, 10], e.g., GrabCut that is an extension of the GraphCut developed by Rother et al [11]. Grady and Funka-Lea [12] have presented Random Walker algorithm based on probabilistic approach. The GrowCut method, developed by Vezhnevets and Konouchine [13], is a cellular automaton-based algorithm for interactive multi label segmentation of N-dimensional images. Zhu et al. [14] reformulates the GrowCut algorithm as a clustering problem and compute a fast approximate solution. This method, called fast GrowCut, is freely available as a module for the medical image computing platform 3D Slicer[15].

Among these algorithms, the level set approach is popular because of its flexibility and robustness. The level set approaches begin with a user-placed seed region of interest (ROI). The algorithm then iteratively deforms the seed ROI to encompass the entire related area. In addition to the seed region, several algorithm parameters explicitly and intrinsically control the growth and smoothness of the ROI surface. These may include the relative weights of external forces acting on the contour, intensity threshold(s), and a surface smoothness parameter [16]. The popularity of this method is increased, because it can handle complex geometries and topological changes. In fact, the level set is a shape-driven tool with a properly defined speed function which can grow or shrink to take the shape of any complex object of interest. The level set method is also an attractive and flexible method for shape modeling and object detection. Another advantage of the level set approach is that given an initial zero level set (initial surface), the entire segmentation procedure is fully automatic. These properties make the level set method a state of the art method for segmentation [2].

One of the main parameters in the level set equation is the speed function, whose design is perhaps the most important step in the level set approach. Threshold-based level set method was first proposed by Lefohn et al. [17] for medical image segmentation. In [18, 19], this method was used to perform segmentation of anatomical structures. Hsu et al. [20] used this method for detecting the boundaries of multiple regions of interest in non-medical images.

In this paper, we proposed a semi-automatic combined level set method based on the combination of region and boundary information in the speed function, to achieve better accuracy in GBM brain tumor segmentation. Also, our method incorporates a fast marching method [21] to form an initial for GBM region based on multiple seed points selected by the user.

II. METHOD AND MATERIALS

A. Materials

To evaluate and compare our algorithm with the others, our experiments were carried out on data set of 6 patients. The dataset contains the MR images of patients with GBM that were acquired at the Sina Specialized & Subspecialty Hospital. MR imaging was performed on 1.5T Siemens devices. Scan parameters were TR = 500ms, TE = 15ms. Table.1 describes the details of the dataset.

TABLE I. Images specification

Patient number	Section	Size (Pixel)	Resolution (mm)
1	axial	512 × 352	0.52 × 0.52
2	sagittal	448 × 512	0.52 × 0.52
3	axial	512 × 352	0.52 × 0.52
4	sagittal	512 × 448	0.52 × 0.52
5	axial	512 × 352	0.52 × 0.52
6	coronal	256 × 176	0.52 × 0.52

We used T1-weighted contrast-enhanced sequence images. In this sequence, brain tumor borders appear brighter because the contrast agent accumulates there due to the disruption of the blood-brain barrier in the proliferative brain tumor region [22]. Also, we choose GBM images with ambiguous borders between surrounding normal brain tissues and edges of tumors.

B. Initial tumor region formation

Multiple points are selected as seed points by physician over the tumor region, including the area near the active tumor boundary, especially the blur edges.

A fast marching level set method was utilized to form an initial tumor region. The speed of fast marching is always non negative and depends on the position of seed points only. It results in an approximate distance function from the initial seed points.

C. Level Set

The initial tumor region formed in the previous section was propagated by the level set method to obtain active tumor region. The level set method evolves a contour implicitly by manipulating a higher dimensional function, called the level set function $\varphi(x, y, t)$. The evolving contour was embedded as the zero level set $\varphi(x, y, t = 0)$. A wide variety of deformations can execute by

introducing an appropriate speed function [16]. The level set evolution equation is defined as:

$$\frac{\partial \varphi}{\partial t} = F|\nabla \varphi| \quad (1)$$

where F is the speed function which controls the propagation of the contour and defined as:

$$F = \alpha D(I) + (1-\alpha)\nabla.\frac{\nabla \varphi}{|\nabla \varphi|} \quad (2)$$

where D is a data term that forces the model toward desirable features in the input data. The term $\nabla.\nabla\varphi/|\nabla\varphi|$ is the mean curvature of the surface, which controls the smoothness of the extracted tumor region and $\alpha \in [0,1]$ is a free parameter that controls the degree of smoothness in the solution.

The data function D in the level set acts as the principal force that drives the segmentation. The strategy is to construct a data term D that causes the contour to grow in regions where the data is consistent with the desired segmentation and to contract in regions where it is not. This was achieved by letting D have positive or negative values. Threshold-based level set method is one of the most common methods of this framework which utilized in many literatures. It is notable that this method has the simple speed function based solely on the input intensity at any one pixel, that is called $D_{threshold}$, given by:

$$D_{threshold}(I) = \begin{cases} I - L & if \quad I < \dfrac{L+U}{2} \\ U - I & if \quad I > \dfrac{L+U}{2} \end{cases} \quad (3)$$

where I is the image intensity and L and U describes the lower threshold and the upper threshold, respectively, which determine experimentally. Upper threshold and lower threshold were examined in reasonable range with consideration of information from image histogram and then we set the optimal value of this range according to results. The propagation term makes the evolving contour enclose pixels, whose intensities are in the threshold interval [L, U].

D. Modified speed function

In our combined method, the data term at any one pixel is the result of the weighted summation of two term: $D_{threshold}$ and $D_{laplacian}$, as below:

$$F = \alpha[\beta D_{threshold}(I) + \gamma D_{laplacian}(I)] + (1-\alpha)\nabla.\frac{\nabla \varphi}{|\nabla \varphi|} \quad (4)$$

β and γ describe the weight of threshold term and Laplacian term, respectively. The second term $D_{laplacian}$ describes the second spatial derivative of an image. The Laplacian of an image highlights regions of rapid intensity change and is therefore often used for edge detection. This term makes the algorithm sensitive to boundaries and led to stop contour's growing around active tumor boundaries. $D_{laplacian}$ is given by:

$$D_{laplacian}(I) = I * \eta \quad (5)$$

Where η is the Laplacian mask that is given by:

$$\eta = \begin{bmatrix} \eta_1 & \eta_2 & \eta_3 \\ \eta_4 & \eta_5 & \eta_6 \\ \eta_7 & \eta_8 & \eta_9 \end{bmatrix} \quad (6)$$

Coefficients are a tightest-fitting convolution kernel which computed as shown below [23]:

$$\begin{aligned} &\eta_1, \eta_3, \eta_7, \eta_9 = 0 \\ &\eta_2, \eta_4, \eta_6, \eta_8 = \left(\frac{1}{h}\right)^2 \\ &\eta_5 = -\sum_{9, i\neq 5}^{i=1} \eta_i \end{aligned} \quad (7)$$

Where h describes the spacing of the input image.

Fig.2 shows a block diagram of our combined method considering threshold parameters, outputs of fast marching and image's Laplacian as inputs of the level set method which is followed by morphological post processing.

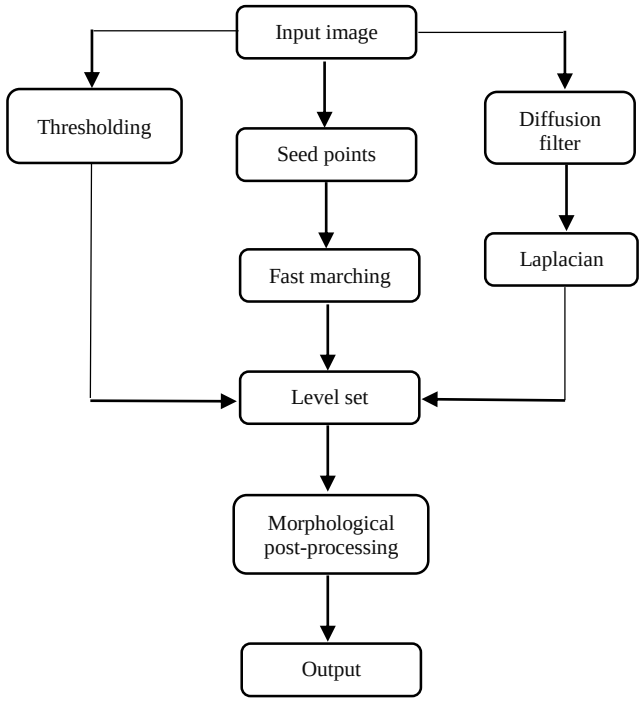

Figure.2 Block diagram of the combined method

Notice that an anisotropic diffusion filter [24] was employed to reduce the effect of noise while preserving the boundaries and fine details. The parameters of the anisotropic diffusion method used in the present study were the number of iterations = 4, time step = 0.06 and conductance parameter = 5.

E. Morphological post-processing

Fill hole algorithm [25] is used to extract whole tumor regions (consist of necrosis and active tumor region, according to Fig.1) from tumor boundary and preparing the result to compare and evaluate the accuracy of tumor segmentation.

III. RESULTS

Our experiments were carried out on real data from 6 patients. Three measures (a) Dice (%), (b) false positive error (FPE %), (c) false negative error (FNE %) were employed for evaluation of accuracy. The accuracy of tumor segmentation was assessed using the Dice coefficient to quantify the overlap between the semi-automatic and the manual segmentation:

$$Dice = 2\frac{|P_{semi-automatic} \cap P_{manual}|}{|P_{semi-automatic}| + |P_{manual}|} \times 100\% \quad (8)$$

where $P_{semi-automatic}$ is the set of semi-automatically extracted pixels and P_{manual} is the set of manually extracted pixels.

FPE is defined as the ratio of the total number of semi-automatically extracted pixels outside the manually extracted tumor region to the total number of manually extracted pixels [26]:

$$FPE = \frac{|P_{semi-automatic}| - |P_{semi-automatic} \cap P_{manual}|}{|P_{manual}|} \times 100\% \quad (9)$$

FNE is the ratio of the total number of manually extracted pixels outside the extracted tumor region to the total number of manually extracted pixels [26]:

$$FNE = \frac{|P_{manual}| - |P_{semi-automatic} \cap P_{manual}|}{|P_{manual}|} \times 100\% \quad (10)$$

The performance of combined method was compared with traditional threshold-based level set method and evaluated with the corresponding tumor region manually traced by a Surgeon from Sina Specialized & Subspecialty Hospital. The GBM regions manually extracted using ITK-Snap [7] were considered as reference segmentation for accuracy evaluation.

The optimal number of seed points was found experimentally by considering the complexity and spread of tumor. The magnitude of lower and upper threshold was determined based on the image histogram information.

Table.2 shows a comparison between our combined method and the traditional method by three measures that mentioned above. Notice that the type of our images is 2 bytes.

Also in Fig.3 and Fig.4 examples of GBM brain tumor segmentation for patient #3 and patient #2 with two methods, combined method and traditional threshold based level set method were shown. β and γ were set to 0.34 and 0.66, respectively, and the weight α of the curvature was determined as 0.95 [20].

The algorithms were implemented by ITK [23] and visualized by VTK and tested on a computer with Core(TM)2 quad CPU 2.66 GHz and 4GB RAM.

IV. CONCLUSION

We have proposed a modified speed function in the level set method, which includes region and boundary information to achieve better accuracy in GBM brain tumor segmentation. In following, it incorporates a fast marching method to form an initial from multiple seed points for active tumor region. Compared to the traditional threshold-based level set method, our combined level set based method is more suited to extract the tumor region precisely. Unlike the traditional method which is only based on region information our combined method is more sensitive to boundaries by utilizing the Laplacian function to highlight fine details.

According to table.2 FPE and FNE were obtained 45.47% and 9.91% in the traditional method, respectively, which indicate a major source of error in this method is related to FPE. In our method by incorporating Laplacian term, the information about rapid intensity change was considered in speed function and led to stop contour's growing around active tumor boundaries. The validation of our experiment represents that the mean of FPE decreased from 45.47% to 21.1%. Also the mean of FNE decreased from 9.91% to 4.64%. The maximum of FPE by using traditional method was related to patient #4 which is improved by 67% in our combined method.

The validation of results for the data of 6 patients indicates that in all the cases we have reached to a reasonable degree of Dice coefficient improvement. The mean of Dice for all patients increased from 76.41% to 88.19%. In the cases 5 and case 3, we reached to the minimum improvement of 7% and maximum 27% dice improvement, respectively.

It is notable that although by incorporating the Laplacian term our results improved significantly, but we are working on advanced edge detectors to make our combined method stronger.

Finally, by using this combined method to segment GBM brain tumor, we are able to achieve better accuracy of segmentation by minimal user interaction which is robust to change of parameters.

ACKNOWLEDGMENT

The study was supported by Image Guided Surgery laboratory at Tehran University of Medical Science. The authors would like to thank Mr. A. Ramzgooyan for his grateful help in writing this paper. This work was supported by the medical school, Tehran University of Medical Science in grant number 29813.

TABLE II. Comparison between traditional method and combined method for 6 patients

Patient number	Number of seed points	Lower threshold	Upper threshold	FPE (%)		FNE (%)		Dice (%)	
				traditional method	combined method	traditional method	combined method	traditional method	combined method
1	24	360	650	37.79	13.25	0.61	1.16	83.81	93.21
2	16	340	650	36.89	16.19	8.37	3.21	80.20	90.89
3	25	355	650	48.12	15.73	19.31	6.2	70.53	89.53
4	16	310	450	52.45	17.09	10.06	9.51	74.21	87.18
5	24	365	660	48.87	32.17	1.28	0.76	79.74	85.77
6	22	370	550	48.75	32.20	19.88	7.05	70.01	82.56
Mean ± std				**45.47± 6.49**	**21.10± 8.67**	**9.91± 8.37**	**4.64± 3.49**	**76.41± 5.66**	**88.19± 3.81**

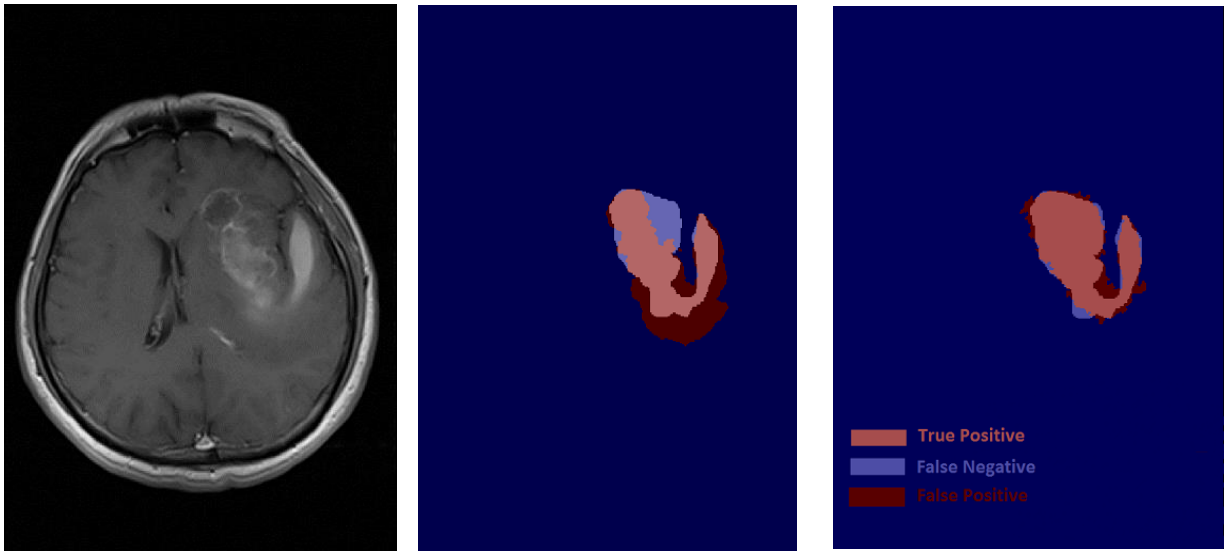

(a) contrast-enhanced T1- weighted MR image (b) GBM segmentation with traditional method (c) GBM segmentation with combined method

Figure 3. Example of GBM segmentation for patient # 3 with two methods

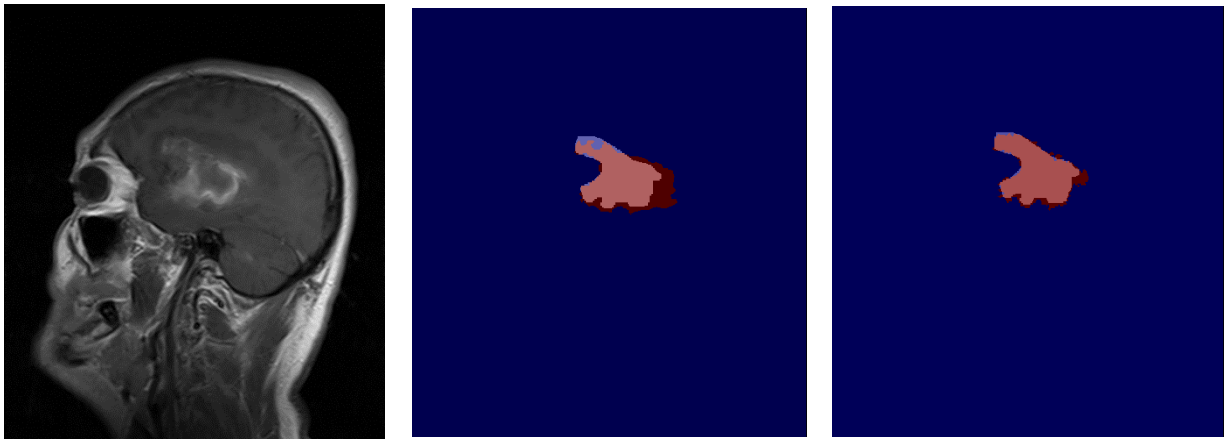

(a) contrast-enhanced T1- weighted MR image (b) GBM segmentation with traditional method (c) GBM segmentation with combined method

Figure 4. Example of GBM segmentation for patient # 2 with two methods

REFERENCES

[1] H. Khotanlou, O. Colliot, J. Atif, and I. Bloch, "3D brain tumor segmentation in MRI using fuzzy classification, symmetry analysis and spatially constrained deformable models," Fuzzy sets and systems, vol. 160, pp. 1457-1473, 2009.

[2] S. Taheri, S. H. Ong, and V. Chong, "Level-set segmentation of brain tumors using a threshold-based speed function," Image and Vision Computing, vol. 28, pp. 26-37, 2010.

[3] C. P. Haar, P. Hebbar, G. C. Wallace, A. Das, W. A. Vandergrift, J. A. Smith, et al., "Drug resistance in glioblastoma: a mini review," Neurochemical research, vol. 37, pp. 1192-1200, 2012.

[4] Q. T. Ostrom, H. Gittleman, J. Xu, C. Kromer, Y. Wolinsky, C. Kruchko, et al., "CBTRUS Statistical Report: Primary Brain and Other Central Nervous System Tumors Diagnosed in the United States in 2009–2013," Neuro-Oncology, vol. 18, pp. v1-v75, 2016.

[5] N. Gordillo, E. Montseny, and P. Sobrevilla, "State of the art survey on MRI brain tumor segmentation," Magnetic resonance imaging, vol. 31, pp. 1426-1438, 2013.

[6] K. Xie, J. Yang, Z. Zhang, and Y. Zhu, "Semi-automated brain tumor and edema segmentation using MRI," European Journal of Radiology, vol. 56, pp. 12-19, 2005.

[7] P. A. Yushkevich, J. Piven, H. C. Hazlett, R. G. Smith, S. Ho, J. C. Gee, et al., "User-guided 3D active contour segmentation of anatomical structures: significantly improved efficiency and reliability," Neuroimage, vol. 31, pp. 1116-1128, 2006.

[8] Y. Y. Boykov and M.-P. Jolly, "Interactive graph cuts for optimal boundary & region segmentation of objects in ND images," in Computer Vision, 2001. ICCV 2001. Proceedings. Eighth IEEE International Conference on, 2001, pp. 105-112.

[9] D. Freedman and T. Zhang, "Interactive graph cut based segmentation with shape priors," in Computer Vision and Pattern Recognition, 2005. CVPR 2005. IEEE Computer Society Conference on, 2005, pp. 755-762.

[10] J. Zhou, M. Ye, and X. Zhang, "Graph cut segmentation with automatic editing for Industrial images," in Intelligent Control and Information Processing (ICICIP), 2010 International Conference on, 2010, pp. 633-637.

[11] C. Rother, V. Kolmogorov, and A. Blake, "Grabcut: Interactive foreground extraction using iterated graph cuts," in ACM transactions on graphics (TOG), 2004, pp. 309-314.

[12] L. Grady and G. Funka-Lea, "Multi-label image segmentation for medical applications based on graph-theoretic electrical potentials," in Computer Vision and Mathematical Methods in Medical and Biomedical Image Analysis, ed: Springer, 2004, pp. 230-245.

[13] V. Vezhnevets and V. Konouchine, "GrowCut: Interactive multi-label ND image segmentation by cellular automata," in proc. of Graphicon, 2005, pp. 150-156.

[14] L. Zhu, I. Kolesov, Y. Gao, R. Kikinis, and A. Tannenbaum, "An effective interactive medical image segmentation method using fast growcut," in MICCAI Workshop on Interactive Medical Image Computing, 2014.

[15] A. Fedorov, R. Beichel, J. Kalpathy-Cramer, J. Finet, J.-C. Fillion-Robin, S. Pujol, et al., "3D Slicer as an image computing platform for the Quantitative Imaging Network," Magnetic resonance imaging, vol. 30, pp. 1323-1341, 2012.

[16] S. Osher and J. A. Sethian, "Fronts propagating with curvature-dependent speed: algorithms based on Hamilton-Jacobi formulations," Journal of computational physics, vol. 79, pp. 12-49, 1988.

[17] A. Lefohn, J. Cates, and R. Whitaker, "Interactive, GPU-based level sets for 3D brain tumor segmentation: Supplementary information," ed, 2003.

[18] P. Parascandolo, L. Cesario, L. Vosilla, M. Pitikakis, and G. Viano, "Smart brush: a real time segmentation tool for 3D medical images," in Image and Signal Processing and Analysis (ISPA), 2013 8th International Symposium on, 2013, pp. 689-694.

[19] X. Yang, H. C. Yu, Y. Choi, W. Lee, B. Wang, J. Yang, et al., "A hybrid semi-automatic method for liver segmentation based on level-set methods using multiple seed points," Computer methods and programs in biomedicine, vol. 113, pp. 69-79, 2014.

[20] C.-Y. Hsu, C.-H. Yang, and H.-C. Wang, "Multi-threshold level set model for image segmentation," EURASIP Journal on Advances in Signal Processing, vol. 2010, p. 40, 2010.

[21] J. A. Sethian, "A fast marching level set method for monotonically advancing fronts," Proceedings of the National Academy of Sciences, vol. 93, pp. 1591-1595, 1996.

[22] J. Liu, M. Li, J. Wang, F. Wu, T. Liu, and Y. Pan, "A survey of MRI-based brain tumor segmentation methods," Tsinghua Science and Technology, vol. 19, pp. 578-595, 2014.

[23] L. Ibanez, W. Schroeder, L. Ng, and J. Cates, "The ITK software guide," 2005.

[24] P. Perona and J. Malik, "Scale-space and edge detection using anisotropic diffusion," IEEE Transactions on pattern analysis and machine intelligence, vol. 12, pp. 629-639, 1990.

[25] P. Soille, Morphological image analysis: principles and applications: Springer Science & Business Media, 2013.

[26] A. Klein, J. Andersson, B. A. Ardekani, J. Ashburner, B. Avants, M.-C. Chiang, et al., "Evaluation of 14 nonlinear deformation algorithms applied to human brain MRI registration," Neuroimage, vol. 46, pp. 786-802, 2009.